Journal of Power Sources 213 (2012) 229–232

Contents lists available at SciVerse ScienceDirect

Journal of Power Sources

journal homepage: www.elsevier.com/locate/jpowsour

Short communication

Magnesiothermically reduced diatomaceous earth as a porous silicon anode material for lithium ion batteries

Lanyao Shen, Xianwei Guo, Xiangpeng Fang, Zhaoxiang Wang*, Liquan Chen

Key Laboratory for Renewable Energy, Beijing Key Laboratory for New Energy Materials and Devices, Beijing National Laboratory for Condense Matter Physics, Institute of Physics, Chinese Academy of Sciences, Beijing 100190, China

ARTICLE INFO

Article history:
Received 7 February 2012
Received in revised form
27 March 2012
Accepted 30 March 2012
Available online 19 April 2012

Keywords:
Porous silicon
Anode
Lithium ion batteries
Diatomaceous earth

ABSTRACT

Three-dimensional porous silicon has been prepared by magnesiothermically reducing diatomaceous earth. BET surface area analysis shows that the specific surface area of the obtained porous silicon is about 96 $m^2\ g^{-1}$, much higher than that of the diatomaceous earth (6 $m^2\ g^{-1}$). The silicon products after HCl immersion have a porous structure similar to that of the diatomaceous earth, with pore sizes around 200 nm. Galvanostatic cycling tests show that the initial charge and discharge capacities of the porous silicon are 1321 mAh g^{-1} and 1818 mAh g^{-1}, respectively. A reversible capacity of 633 mAh g^{-1} is retained after 30 cycles.

1. Introduction

Lithium ion batteries are the most popular power sources in portable electric and electronic devices for their advantages such as high power and energy densities and environmental friendliness. Much effort is now being paid to replace the commercially used graphite with materials with higher specific lithium storage capacity and higher safety [1]. Silicon is one of the most attractive anode materials for its large specific capacity (theoretically 4200 mAh g^{-1}) [2] and its lithium insertion potential properly above that of lithium deposition. However, the severe pulverization of the Si particles due to volume change during cycling destroys the electric conducting network and results in rapid capacity fading.

To improve the cyclability of Si-based anodes materials, several methods have been exploited, such as reducing the Si particle size to nanometer scales [3], dispersing the particles in an inactive or active matrix [4], and reforming the morphology of silicon-based anodes [5–7]. Among these strategies, constructing Si-based materials with porous structure has been proved effective [6,8]. The void space in the porous Si can partially accommodate the huge volume change during the charge and discharge process and facilitate the transportation of lithium ions [9].

Recently, Yu et al. [10] and Jia et al. [11] synthesized 3D porous silicon using a magnesiothermic method by the equation $2\ Mg + SiO_2 \rightarrow 2MgO + Si$, with mesoporous silica (SBA-15) as the Si source and template. However, as the SBA-15 template is expensive, it cannot be cost-effective to use such material as the source of silicon. On the other hand, diatomaceous earth is a biogenic siliceous sedimentary rock; its main component is silica. It is very cheap and commercially available. Bao et al. [12] reported that porous silicon can be obtained by a magnesiothermic reduction of diatomaceous earth at low temperature (650 °C). The natural porous structure of diatomaceous earth works as another kind of template for porous silicon. However, their work was only focused on the conversion of three-dimensional silica into microporous silicon replicas. They did not evaluate the electrochemical performances of the reduced product.

In this work, porous silicon was synthesized by magnesiothermically reducing the diatomaceous earth as the silicon source and template. The reduction product was then coated with a layer of carbon to enhance its electric conductivity. Electrochemical evaluation indicates that the diatomaceous earth could be a promising precursor of porous silicon anode material.

2. Experimental

The diatomaceous earth was reduced by a magnesiothermic reduction. In a typical process, 0.6 g diatomaceous earth (CP) and 0.6 g Mg powder (AR, 100–200 mesh) was mixed and ground in an

* Corresponding author. Tel./fax: +86 10 82649050.
E-mail address: zxwang@iphy.ac.cn (Z. Wang).

0378-7753/$ – see front matter © 2012 Elsevier B.V. All rights reserved.
doi:10.1016/j.jpowsour.2012.03.097

agate mortar for 20 min. Then the mixture was annealed in a tube furnace at 650 °C for 6 h under Ar/H_2 (92:8 v/v) atmosphere at a ramping rate of 5 °C min^{-1}. The obtained powder was immersed in 200 ml, 0.5 M HCl solution for 12 h, rinsed with distilled water and ethanol several times to remove the MgO. After centrifugation, the powder was vacuum-dried at 80 °C for 10 h. To coat the obtained porous silicon with carbon, 0.25 g porous silicon was heat-treated in an argon/toluene mixed atmosphere in a tube furnace at 800 °C for 6 h. Carbon-coated silicon (Si/C) composite was obtained after the furnace was naturally cooled down to room temperature in Ar.

The structure and specific surface area of the diatomaceous earth and porous silicon was characterized by X-ray diffraction (X'Pert Pro MPD X-ray diffractometer, Philips, Holland) using Cu Kα radiation and Brunauer-Emmett-Teller method (NOVA 2000e surface area analyzer, Quanta-chrome Instruments). Raman spectroscopy (Renishaw inVia micro-Raman spectroscopy system equipped with a 514.5 nm laser) was used to investigate the structure of the reduced diatomaceous earth and the existence of carbon of the sample after carbon coating. Scanning electron microscopy (XL 30 S-FEG, FEI Co.) was applied to study the morphology of the diatomaceous earth and porous silicon.

Electrochemical tests were performed using two-electrode Swagelok-type cells. The working electrode was prepared by casting a mixture of 75 wt% active material (Si/C composite), 15 wt% carbon black and 10 wt% sodium alginate binder on a copper current collector. The counter electrode was a fresh lithium foil. The cell was assembled in an Ar-filled glove box with Celegard 2400 as the separator and 1 M $LiPF_6$ in ethylene carbonate (EC) and dimethyl carbonate (DMC) (1:1 by volume) as the electrolyte with VC additives (2 wt%). The cells were charged and discharged between 0.01 and 1.5 V at room temperature on a Land battery tester (Wuhan, China).

3. Results and discussion

The morphology of the diatomaceous earth before and after magnesiothermic reduction is compared in Fig. 1. The commercial diatomaceous earth is sunflower-like with particle size of about 25 μm and uniform pore size of about 200 nm (Fig. 1a). The shape of the sunflower was damaged after magnesiothermic reduction and HCl immersion. The size of the obtained porous Si particles decreases to less than 10 μm though the pore size remains about 200 nm. This indicates that magnesiothermic reduction does not

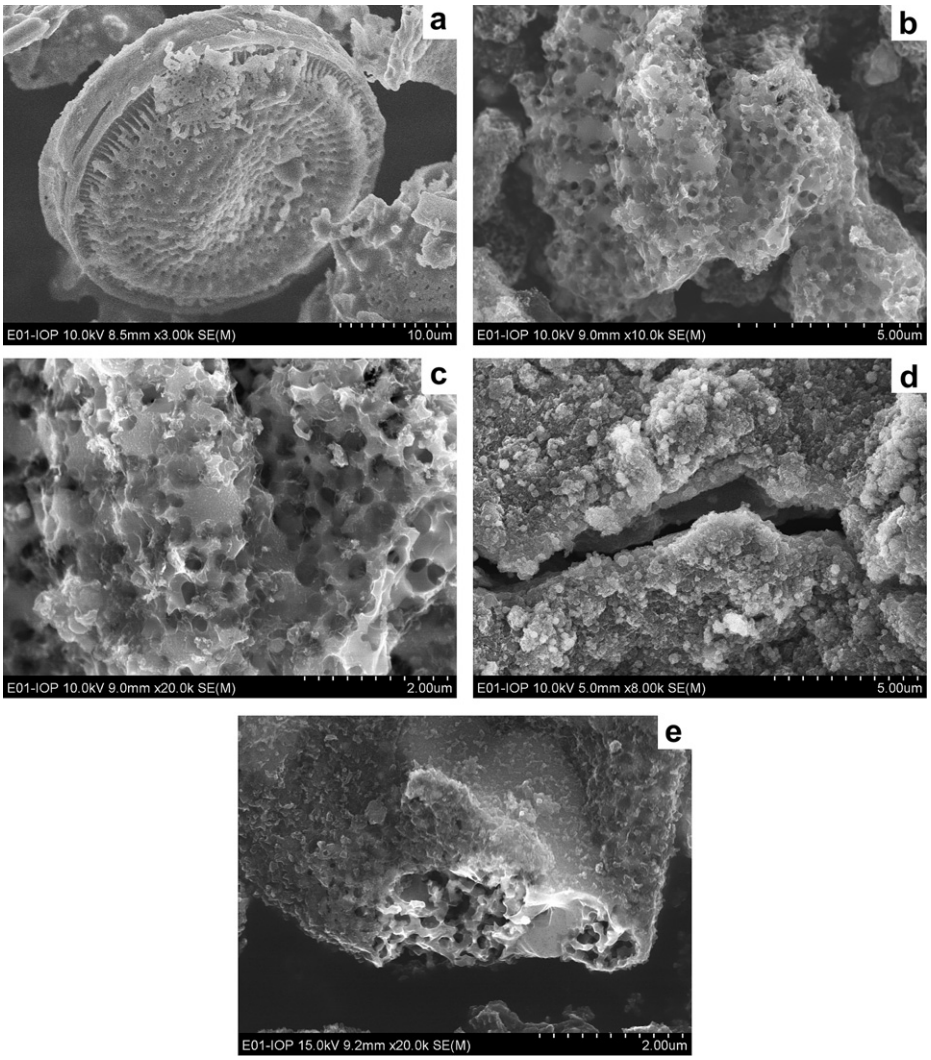

Fig. 1. Morphology of the as-received diatomaceous earth (a), magnesiothermically obtained porous silicon (b and c), the porous silicon electrode after 30 galvanostatic cycles (d) and carbon-coated porous silicon (e).

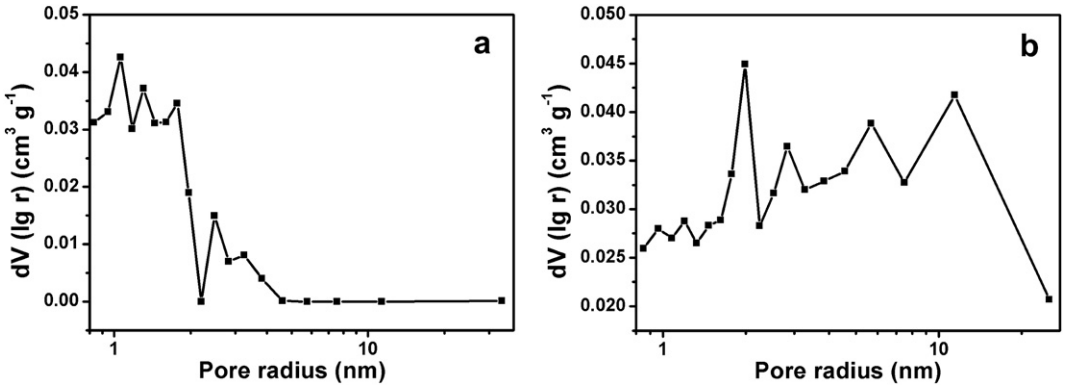

Fig. 2. The pore size distribution of the diatomaceous earth (a) and porous silicon (b) calculated by BJH formula in the desorption branch isotherm.

damage the porous structure of the diatomaceous earth. In this sense, the diatomaceous earth works as a template of porous silicon.

The specific surface area of the reduced diatomaceous earth was determined to be 96 $m^2\ g^{-1}$ by the Brunauer-Emmett-Teller (BET) method, much higher than that of the as-received diatomaceous earth (6 $m^2\ g^{-1}$). The analysis of the size of the micro-pores (Fig. 2) indicates that the diameters of micro-pores increase after the magnesiothermic reduction. Combined with the value of the BET surface area, mesopores are believed to be created during the magnesiothermic reduction due to the formation of MgO and its removal by HCl.

The XRD patterns of the diatomaceous earth before and after magnesiothermic reduction are shown in Fig. 3. The intense peak is indexed as the (101) face of tetragonal silica (P41212 space group; JCPDS 76–0940). The main composition of the as-received diatomaceous earth is SiO_2. Fig. 3b shows that Si is obtained after magnesiothermic reduction and HCl immersion. All the indexed peaks are consistent with that of the cubic silicon (JCPDS 26–1481). Inductively coupled plasma (ICP) analysis shows that the content of silicon in the HCl-immersed sample is 85 wt%.

To improve the electric contact and the electronic conductivity of the porous silicon, a layer of amorphous carbon is coated onto the silicon replica by chemical vapor deposition (CVD) method (Fig. 1e). The presence of the peaks at 1340 cm^{-1} and 1589 cm^{-1} (referred as the D- and *G*-bands of carbon, respectively) in the Raman spectrum demonstrates the amorphous feature of the deposited carbon. In addition, it was reported that the strongest Raman peak of SiO_2 is located at 440 cm^{-1} [13]. Therefore, the presence of a negligible peak in the Raman spectra with high signal/noise ratio (Fig. 3c) indicates that there is some trace of SiO_2 in the porous Si. This explains the low content of Si in the porous Si (that is, there is still some oxygen in the porous silicon. Other elements include Ca, Fe, Mg and Al, all below 1 wt%). All the other Raman peaks below 1000 cm^{-1} in the spectra can be attributed to silicon [14]. As XRD is sensitive to the crystalline while Raman spectroscopy is sensitive to both the amorphous and crystalline phases, the Raman spectra actually demonstrate the diatomaceous earth has been transformed to porous silicon after magnesiothermic reduction.

Fig. 4a shows the voltage profiles of the carbon-coated porous silicon cycled between 0.01 and 1.5 V at a galvanostatic current density of 0.2 mA cm^{-2}. The first charge and discharge capacities of the sample are 1321 mAh g^{-1} and 1818 mAh g^{-1}, respectively (coulombic efficiency 73%). The irreversible capacity is attributed to the formation of the solid electrolyte interphase (SEI) layer during the first discharge process and the trapping of the lithium ions in the defected and pulverized silicon particles. A small hump appears at the beginning of the first discharge profile. A charge capacity increase is observed in the second charging process, indicating the existence of an activation process. The entrance of the organic electrolyte into the micro-pores of the porous silicon might be responsible to this activation process because much time is required for the large organic electrolyte molecules to go into the micro-pores of the porous silicon. However, the initial discharge induces the particle pulverization, helping the electrolyte to enter the pores and more of the active material can be used, resulting in a temporary capacity increase. Fig. 4b displays the cyclability of the porous silicon and carbon-coated porous

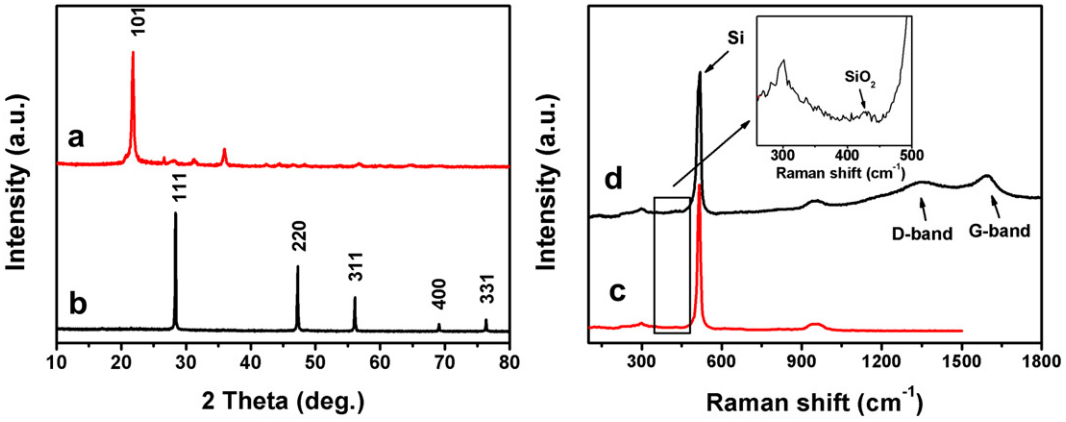

Fig. 3. The X-ray diffraction patterns of the diatomaceous earth (a) and the porous silicon (b) and the Raman spectra of porous silicon before (c) and after (d) Carbon coating. The inset is for the selected Raman spectrum of both (c) and (d) between 260 and 500 cm^{-1}.

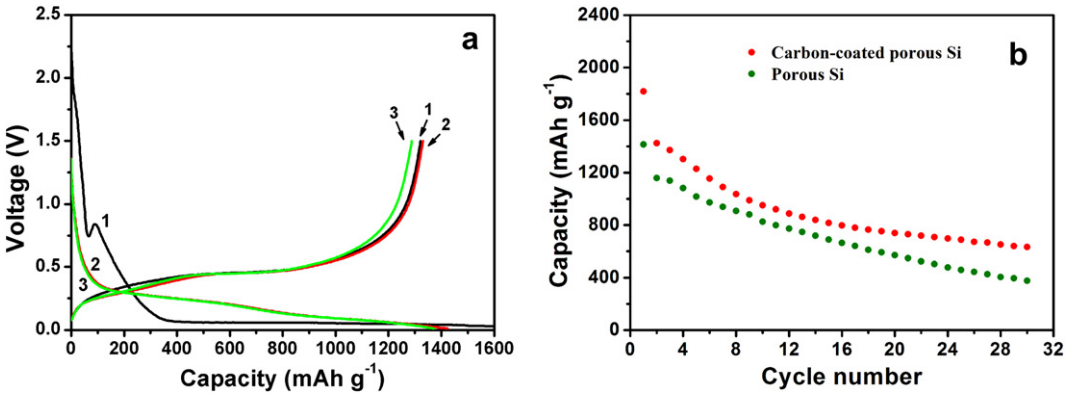

Fig. 4. The voltage profiles of the carbon-coated porous silicon (a) and comparison of the cycling performances (b) of the porous silicon and carbon-coated porous silicon electrode between 0.01 and 1.5 V at a current density of 0.2 mA cm^{-2}.

silicon. A reversible capacity of 633 mAh g^{-1} is still obtained after 30 cycles for the carbon-coated porous silicon while that of the carbon-free porous silicon electrode is 376 mAh g^{-1}. The good cycling stability is attributed to the improved electric contact and surface electronic conductivity by the amorphous carbon coating layer. However, the particle pulverization of the active materials is not completely avoided, leading to the capacity decay in the subsequent charge and discharge processes. Fig. 1d shows that obvious cracks can still be observed on the electrode materials after 30 cycles. The cracks not only destroy the structure of the electrode material, but also increase the surface area of the active material, resulting in low coulombic efficiency. Further optimization of the electrode material, including the decrease of the particle size and the distribution of the pores, is needed to improve the electrochemical performance of porous silicon.

4. Conclusion

Porous silicon replica has been prepared by magnesiothermically reducing diatomaceous earth. After carbon coating by the CVD method, this material shows excellent good lithium storage performance and capacity retention. Although further work is necessary to improve the capacity retention of the sample, these results demonstrate the feasibility of using the magnesiothermically reduced diatomaceous earth as a promising porous silicon anode material.

Acknowledgments

This work was financially supported by the National 973 Program (2009CB220100) and the National Science Foundation of China (NSFC, 50472072 and 20974120).

References

[1] M. Holzapfel, H. Buqa, L.J. Hardwick, M. Hahn, A. Würsig, W. Scheifele, P. Novák, R. Kötz, C. Veit, F.-M. Petrat, Electrochim. Acta 52 (2006) 973–978.
[2] B.A. Boukamp, G.C. Lesh, R.A. Huggins, J. Electrochem Soc. 128 (1981) 725–729.
[3] U. Kasavajjula, C. Wang, A.J. Appleby, J. Power Sources 163 (2007) 1003–1039.
[4] H. Li, X.J. Huang, L.Q. Chen, Z.G. Wu, Y. Liang, Electrochem Solid St. 2 (1999) 547–549.
[5] H. Ma, F.Y. Cheng, J. Chen, J.Z. Zhao, C.S. Li, Z.L. Tao, J. Liang, Adv. Mater. 19 (2007) 4067–4070.
[6] A. Esmanski, G.A. Ozin, Adv. Funct. Mater. 19 (2009) 1999–2010.
[7] A. Magasinski, P. Dixon, B. Hertzberg, A. Kvit, J. Ayala, G. Yushin, Nat. Mater. 9 (2010) 353–358.
[8] H.C. Shin, J.A. Corno, J.L. Gole, M.L. Liu, J. Power Sources 139 (2005) 314–320.
[9] H. Kim, B. Han, J. Choo, J. Cho, Angew. Chem.-Int. Edit. 47 (2008) 10151–10154.
[10] Y. Yu, L. Gu, C. Zhu, S. Tsukimoto, P.A. van Aken, J. Maier, Adv. Mater. 22 (2010) 2247–2250.
[11] H. Jia, P. Gao, J. Yang, J. Wang, Y. Nuli, Z. Yang, Adv. Energy Mater. 1 (2011) 1036–1039.
[12] Z.H. Bao, M.R. Weatherspoon, S. Shian, Y. Cai, P.D. Graham, S.M. Allan, G. Ahmad, M.B. Dickerson, B.C. Church, Z.T. Kang, H.W. Abernathy, C.J. Summers, M.L. Liu, K.H. Sandhage, Nature 446 (2007) 172–175.
[13] R.J. Hemley, H.K. Mao, P.M. Bell, B.O. Mysen, Phys. Rev. Lett. 57 (1986) 747–750.
[14] J. Bonse, K.W. Brzezinka, A.J. Meixner, Appl. Surf. Sci. 221 (2004) 215–230.